

Dalton Transactions

Accepted Manuscript



This is an *Accepted Manuscript*, which has been through the Royal Society of Chemistry peer review process and has been accepted for publication.

Accepted Manuscripts are published online shortly after acceptance, before technical editing, formatting and proof reading. Using this free service, authors can make their results available to the community, in citable form, before we publish the edited article. We will replace this *Accepted Manuscript* with the edited and formatted *Advance Article* as soon as it is available.

You can find more information about *Accepted Manuscripts* in the [Information for Authors](#).

Please note that technical editing may introduce minor changes to the text and/or graphics, which may alter content. The journal's standard [Terms & Conditions](#) and the [Ethical guidelines](#) still apply. In no event shall the Royal Society of Chemistry be held responsible for any errors or omissions in this *Accepted Manuscript* or any consequences arising from the use of any information it contains.

Synthesis of an unexpected $[\text{Zn}_2]^{2+}$ species utilizing an MFI-type zeolite as a nano-reaction pot and its manipulation with light and heat

Akira Oda,¹ Takahiro Ohkubo,¹ Takashi Yumura,² Hisayoshi Kobayashi² and Yasushige

Kuroda^{1*}

Compared with mercury, the existence of $[\text{Zn}_2]^{2+}$ species is rare. We succeeded in preparing a stable $[\text{Zn}_2]^{2+}$ species utilizing an MFI-type zeolite as a nano-reaction pot, which was confirmed using XAFS spectroscopy: the bands at $R = 2.35 \text{ \AA}$ due to the Zn^+-Zn^+ scattering and at 9660.7 eV to the $1s-\sigma^*$ (the anti-bonding orbital comprised of the $4s-4s$ orbital) transition of the $[\text{Zn}_2]^{2+}$ species. This species also gives the characteristic band around $42,000 \text{ cm}^{-1}$ due to its $\sigma-\sigma^*$ transition. Furthermore, the UV-irradiation corresponding to the $\sigma-\sigma^*$ transition causes the bond dissociation, forming unprecedented two Zn^+ ions, and detached Zn^+ ions were recombined through the heat-treatment at 573 K: $[\text{Zn}^+-\text{Zn}^+] \rightleftharpoons 2\text{Zn}^+$. These processes were reproduced by applying the DFT calculation method to the assumed triplet, $\sigma(\alpha)-\sigma^*(\alpha)$, structure formed on the M7-S2 site with the specific Al array in the MFI-type zeolite. Research into the specific field using zeolites to synthesize “ultra-state ions” is very promising.

1. Introduction

Group 12 elements have zero- or divalent-state as the normal valence states. Only mercury shows a formal monovalent oxidation state, which is well known and is hitherto of importance in chemistry. It should be noted that mercury exhibits a dimeric state, $[\text{Hg}_2]^{2+}$, even in an aqueous solution.¹ Actually, the formation of dimeric species comprised of Group 12 elements with the monovalent state seems to be energetically favorable on the basis of the concept of the molecular orbital (MO) theory.²⁻

⁴ As for the zinc ion, it is generally accepted that the existence of monovalent species and, of course, of its dimeric species have been known little and even the formation of a single monovalent species is limited to the cases prepared under severe preparation conditions, such as gamma-ray irradiation condition and so on.⁵⁻⁷

In 2012, a stable paramagnetic mononuclear Zn^+ ion was prepared for the first time by Deng et al., utilizing the subnanometer sized space of a zeolite sample.⁸ However, zinc species having metal-metal bond has not been known to form stable homonuclear zinc moieties for a long time, although the possibility of their existence is predicted from the MO theory. It is the 2004 year that Resa et al. have successfully synthesized a dimeric $[Zn_2]^{2+}$ species as a complex and also succeeded in determining the structure of the compound, which was found to be a dinuclear pentamethyl-cyclopentadienyl zinc compound that had a zinc-zinc bond.⁹ This work shed new light on the chemistry of the Group 12 elements, and researches in this field have been progressing ever since this discovery.^{10,11} However, thus prepared samples containing dimeric zinc species are basically unstable by nature. Therefore, despite the researches that have been conducted so far, little is known about electronic nature and reactivity of dimeric $[Zn_2]^{2+}$ species.

Until now, we have focused our attention on the features of the exchanged metal ions arising from the specific reaction field of zeolites with a subnanometer-sized pore. Under such circumstances, we have encountered the fascinating phenomena recently arising from zinc ions grafted into an MFI-type zeolite that has the Si/Al ratio of 11.9.¹²⁻¹⁴ These features show: (1) an unprecedented redox feature of the exchanged zinc ion between divalent and zero-valent states via a ZnH^+ species, (2) the formation of an atomic zinc species and its stabilization through a certain kind of interaction with Brønsted acid site, and (3) the production of a stable Zn^+ species through the UV irradiation onto the atomic Zn^0 species formed.

These features mentioned above are arising from two dominant factors. The first factor is caused by the coordination unsaturation around the exchanged ion, as well as the distorted bond-angle comprised of the $O(L)-M^{2+}-O(L)$ moiety, where O(L) means the lattice oxygen atom connected to an Al atom. The second factor depends on the configuration of the composite Al atoms in the respective

membered rings of the MFI-type zeolite which evokes a marked effect on the electronic nature of the exchanged Zn^{2+} ion. Advantageously, it is fortunate that the melting point of metallic zinc is relatively lower in temperature as that of the metals.¹ Taking these phenomena into consideration, we anticipated that a subnanometer sized reaction pot utilizing zeolite would have the potential to prepare a $[\text{Zn}_2]^{2+}$ species through a solid ion-exchanging method with zeolite having an appropriate Si/Al ratio, as well as the specific Al arrangement, which would also have advantages regarding its spatial and charge compensation characteristics.

In this work, we focused our attention on the possibility of easy preparation of dimeric Zn^+ species utilizing an MFI-type zeolite as a reaction pot with subnanometer sized pore through a solid-vapour reaction utilizing Zn^0 and its formation mechanism, and also intended to clarify the reactivity of the formed dimeric species under UV irradiation, as well as its changing mechanism in the UV irradiation process.

2. Experimental section

Materials: In our experiments, the special-grade reagents used, $\text{Zn}(\text{NO}_3)_2$, powdered Zn, and NH_4NO_3 , were purchased from Nacalai Tesque Co. (Japan). The sodium-type MFI zeolite (NaMFI, Si/Al ratio = 11.9) used was provided by the Tosoh Co., Japan and was converted into an NH_4 -type zeolite (NH_4MFI) via ion exchange in an aqueous ammonium nitrate solution at 313 K for 10 min. This procedure was repeated five times. The prepared NH_4MFI sample was treated in vacuo at 873 K for 5 h to obtain an H-type zeolite (HMFI): $\text{H}_{7.44}\text{Al}_{7.44}\text{Si}_{88.56}\text{O}_{192}$. In this work, the solid ion-exchanging method was used to prepare the samples. In the solid-vapour preparation procedure, 200 mg of the dehydrated HMFI sample was mixed with X mg of Zn powder ($X = 5$ to 15 mg) by using an agate mortar and pestle. After mixing thoroughly in a glove box, the mixed reactants were treated at 673 K under in situ conditions without any exposure to ambient gases. Thus prepared samples were denoted in abbreviated form as $\text{HMFI-Zn}^0\text{-}X$, where X indicates the mass in milligrams of Zn

loading used in the preparation procedure. After the reaction with Zn^0 , the IR band observed at 3615 cm^{-1} which is assignable to the Brønsted acid site in HMFI decreases its intensity, clearly indicating that the substitution reaction of H^+ with some kind of zinc ions (Zn^{2+} or also Zn^+) takes place.

To compare the samples' properties with those of a reference sample, the HMFI sample made was then ion exchanged with Zn^{2+} ions using a conventional ion-exchanging method of submerging the sample in an aqueous solution of zinc(II) nitrate at 300 K for 1 h, denoted as Sample $\text{Zn}^{2+}\text{MFI-95}$.¹²⁻¹⁴ The final number shown in the sample notation indicates the ion exchange capacity that was evaluated by assuming one Zn^{2+} -ion exchange per two protons in MFI.

Methods: We used several experimental methods in this work, such as X-ray absorption fine structure (XAFS), UV-vis diffuse reflectance, and ESR spectroscopy, and also the theoretical method utilizing DFT calculations in our analysis. The UV-vis irradiation experiments were performed under in situ conditions utilizing a 100 W xenon light source (Asahi Spectra, LAX-Cute). Throughout these experiments, we examined the effective wavenumber of the UV light for changing the states of the $[\text{Zn}_2]^{2+}$ species formed. In this case, UV-vis light with different wavenumbers that was regulated by introducing a cutoff filter into the light path was irradiated on Sample HMFI- Zn^0 -15 to examine the role of the triggering electron, which had a marked effect on the dimer species formed.

X-ray absorption fine structure (XAFS) spectra: The K-edge XAFS spectra of zinc (in both the XANES and EXAFS regions) were measured at the BL-9C beamline of the KEK-PF facility (Tsukuba, Japan), which was equipped with a double crystal Si(111) monochromator, under ring operating conditions of 2.5 GeV and 300 mA. In our measurements, a pelletized sample was prepared using the same procedure described in the Materials section and was evacuated at 673 K utilizing an in situ cell. The XAFS data were analyzed using software developed by the Rigaku Co.¹⁵

Diffuse reflectance (DR) spectra: DR spectra in the ultraviolet and visible (UV-vis) regions were recorded at 300 K in the wavenumber range $50,000\text{--}15,000\text{ cm}^{-1}$ using a Jasco spectrophotometer (Model V-570) equipped with an integral sphere attachment to obtain the spectra from the samples. A

powdered sample was placed in a vacuum reflectance cell made of fused silica under an N₂ gas atmosphere. Spectralon (Labsphere, USA) was used as the reference material. In these measurements, the samples were heat-treated in vacuo and also irradiated with UV-vis light under in situ conditions.

Electron Spin Resonance (ESR) spectra: All the ESR measurements were carried out under in situ conditions. The prepared HMFI-Zn⁰-X sample was loaded into a quartz tube in a glove box and successively treated at 673 K in vacuo. The ESR spectra were recorded at the X-band frequency (ca. 9.5 GHz) at 300 K using a JEOL JES-FA-2000 spectrometer. The *g* values were determined by reference to the spectrum of Mn²⁺ doped into MgO as a standard.

Computational Methodology (Calculation method): In the present study, we used one of the most successful hybrid Hatree-Fock/DFT methods, implemented in the Gaussian 09 software package.¹⁶ The B3LYP method^{17–20} was used in our calculations. In general, the hybrid B3LYP method is well known to provide excellent descriptions of various properties.²¹ As a realistic model of an aluminum-free MFI zeolite, we adopted an Si₉₂O₁₅₁H₆₆ cluster model, where the peripheral atoms were terminated with H atoms.²² This model contained the basic part of the MFI framework including a 10-membered ring, 10-MR, explicitly.²³ Using this fundamental MFI zeolite structure, we constructed a ZnMFI model where a single Zn cation was located in the vicinity of two Al atoms substituted for two Si atoms within the 10-MR: ZnAl₂Si₉₀O₁₅₁H₆₆. Previously, our studies confirmed that this B3LYP-optimized MFI zeolite model comprised of 10-MR in cavities reproduced well the experimentally observed data.^{12–14,22,24–31} Taking our previous works into consideration, we used the M7 site for the Al substitution position;³² and we defined the Al configuration as the [M7-S2] arrangement.^{12–14,30} To optimize fully the larger MFI geometry with a 10-MR cavity, we used the 6-311G(d) basis set for the zinc atom and the 6-31G(d) basis set for the Al atom, as well as four O atoms that were connected to the substituted Al atom. The 3-21G basis set was used for Si, H, and other O atoms in the zeolite frameworks. After full optimization, an additional Zn atom was positioned at the distance of 3 Å from the originally inserted Zn²⁺ ion. As the result of the full optimization of this structure, we also evaluated the local states with various Zn-Zn bond distances,

as well as their stabilization energies in the respective states. The stabilization energies were evaluated for the system ($\text{Zn}^0 + \text{Zn}^{2+}\text{MFI}$) with various distances between the Zn atoms, starting 3 Å until the final most stable state was established: $\text{Zn}^0 + \text{Zn}^{2+}\text{MFI} \rightarrow [\text{Zn}_2]^{2+}\text{MFI}$. Additional calculations were also carried out for the site with a different Al arrangement: the [M7-M5] site.

TD-DFT calculations were carried out utilizing the Gaussian 09 software package. We used the LanL2DZ basis set to obtain the photo-absorption spectrum of the $[\text{Zn}_2]^{2+}$ species formed on the M7-S2 model because of the limitations of computational resources, and in addition, we used the M7-M5 model on which the $[\text{Zn}_2]^{2+}$ species was formed. In both cases, we utilized the MFI zeolite structure composed of $\text{Al}_2\text{Si}_{90}\text{O}_{151}\text{H}_{66}$.

3. Results and discussion

3.1 Characterization of a synthesized $[\text{Zn}_2]^{2+}$ species into HMFI.

XAFS spectroscopy is an excellent technique for obtaining information on the coordination structure around a target atom as well as characterizing its electronic nature, and was used to characterize the states of the zinc species in the prepared samples. The X-ray absorption near-edge structure (XANES) spectra of the HMFI- Zn^0 -X samples (where X means the Zn loading in the samples and the detailed definition is given in the experimental section.) are shown in Fig. 1A. The HMFI- Zn^0 -5 sample exhibited characteristic absorption bands at 9663.7 and 9669.7 eV, being attributable to the $1s \rightarrow 4p$ transitions for monomeric Zn^{2+} ions exchanged in the MFI zeolite.^{12,33} The XANES spectrum of Sample HMFI- Zn^0 -5 is consistent with that of Sample Zn^{2+} -MFI (Fig. S1), supporting that the zinc metal-atoms used in the preparation process of the HMFI- Zn^0 -5 sample were quantitatively oxidized to monomeric Zn^{2+} ions. These data clearly show the formation of monomeric Zn^{2+} ions exchanged in the MFI zeolite through a two-electron oxidation of the Zn^0 atoms used in the preparation process with the protons on the Brønsted acid sites, accompanied by the release of an H_2 molecule, as shown in Scheme 1 (a \rightarrow b).³⁴ As evidenced by the marked

weakening of the intensity of the XANES bands at 9663.7 and 9669.7 eV in the spectra with increasing Zn loading, the number of monomeric Zn^{2+} ions exchanged in MFI decreased substantially with increasing Zn^0 loading. It is worth noting that a new, distinct absorption band appeared at 9660.7 eV and its intensity increased with increasing Zn^0 loading. These data can be interpreted that the generated Zn^{2+} ion in the preparation procedure using smaller quantities of Zn^0 reacts with coming additional Zn^0 vapour to form a new zinc species in the samples having higher loading levels of zinc.

The extended XAFS (EXAFS) spectra for the HMFI- Zn^0 - X samples were measured to identify the states of zinc species present, especially for those samples prepared with higher Zn^0 loadings, and these are shown in Fig. 1B. A prominent band at ca. 1.5 Å (no-phase corrected) was distinctly observed in the spectrum of Sample HMFI- Zn^0 -5. Taking account of the fact that dominant zinc species in Sample HMFI- Zn^0 -5 is monomeric Zn^{2+} ions exchanged in MFI, the band at 1.5 Å (not phase corrected) was due to backscattering from the first nearest oxygen atoms surrounding the exchanged Zn ion. In addition to the observation of this band, a discernible band can be recognized at 2.1 Å (not phase corrected). The intensity of the latter band increased with increasing Zn^0 loading, accompanied by an apparent decrease in intensity of the Zn–O band occurring at 1.5 Å. With the above-mentioned XANES data in mind, the band at 2.1 Å is assignable to the Zn^{n+} – Zn^{n+} correlation from a new type of the zinc species formed by the reaction between monomeric Zn^{2+} ions exchanged in MFI and Zn^0 vapour.

On the basis of our proposed idea (the formation of $[\text{Zn}_2]^{2+}$ species), we carried out an EXAFS analysis and evaluated the structural parameters on the first and second shells around a zinc species in HMFI- Zn^0 - X samples. In our analytical procedures, the least-squares method was applied using the scattering parameters obtained from ZnO and Zn^0 foil as the reference materials for the oxygen and zinc atoms around the zinc species, respectively. The Zn K-edge EXAFS curve-fitted results are summarized in Tab. 1 and supplementary Fig. S2. It can be seen that there are two dominant kinds of bands in the Fourier-transformed spectra that were well reproduced using the parameters obtained from reference samples, as shown in supplementary Fig. S2, which strongly supports our band

assignments discussed above. What is important is that the coordination number (CN) of Zn for the second shell is evaluated to be almost one for the HMFI-Zn⁰-15 sample, and the Zn–Zn bond distances is ca. 2.37 Å, which is obviously shorter than twice of the metallic radius of Zn (1.37 Å), and is within the Zn–Zn bond length of the [Zn₂]²⁺ species found in decamethyldizincocene and also that for related compounds (2.30–2.41 Å).^{9,10} Compared with the EXAFS spectrum for Zn foil, which is also given in Fig. S3, the spectra for the HMFI-Zn⁰-X samples clearly suggest the formation of species with a shorter bond length due to the Zn⁺-Zn⁺ correlation in the HMFI-Zn⁰-X samples, which was especially so for samples with a higher concentration of zinc species: Fig. 1B. In addition, it cannot be emphasized too strongly that the CN (coordination number) of zinc in the second shell from our EXAFS analysis affords a linear relationship against the intensity of the XANES band at 9660.7 eV through the origin as shown in Fig. 1C, well supporting our claim that the [Zn₂]²⁺ species is formed by the comproportionation reaction between Zn²⁺ and Zn⁰ as proposed in Scheme 1, (b→c). The newly developed XANES band at 9660.7 eV may be assignable to the 1s→σ* transition in the formed [Zn₂]²⁺ species having the valence electronic configuration of (σ_g)², resulting from the formed [Zn⁺-Zn⁺] species (also compare this with the XANES data of Zn⁰-foil shown in supplementary Fig. S1).

The formation of [Zn₂]²⁺ species, especially at higher Zn⁰ loading levels, was also supported by the data obtained from DR measurements in the UV-Vis region (Fig. 1D). The respective samples display at least two characteristic absorption bands in the ultraviolet region of 50,000 to 30,000 cm⁻¹, in which their intensities increased concurrent with an increase in the Zn⁰ loading. Taking EXAFS data into consideration, the DR bands around at 50000-30000 cm⁻¹ may be assignable to the σ→σ* and/or σ→π_{x,y} electronic transitions of the [Zn₂]²⁺ species formed in the MFI zeolite. The absorption energies obtained experimentally are in accord with the data obtained by the calculations for decamethyldizincocene, which strongly supports our new finding; i.e., the facile formation of [Zn₂]²⁺ species embedded in the MFI-type zeolite.^{35,36}

3.2 Model Studies.

To substantiate the formation of a stable $[\text{Zn}_2]^{2+}$ species embedded in the MFI zeolite, we constructed a $[\text{Zn}_2]^{2+}$ -MFI model with the aid of the density functional theory (DFT) calculation, and tried to reproduce the obtained experimental data utilizing the constructed model. For explaining all data found in this work appropriately, we adopted an optimized $[\text{Zn}_2]^{2+}$ structure using the M7-S2 model as the most reasonable model from several candidate models, in which the $[\text{Zn}_2]^{2+}$ dimeric species was located on the M7 site in the MFI zeolite having a specific configuration comprising two Al atoms (Fig. 2A).^{12-14,22,30} The reason that we chose this model is because it had been confirmed previously that the calculation using this model provides a complete description of the electronic states of a monomeric Zn^{2+} ion embedded in MFI in the activation processes of H_2 or CH_4 activation at temperatures around 300 K, as well as the formation of Zn^+ ion.^{12-14,30} The resulting structural parameters of the optimized $[\text{Zn}_2]^{2+}$ -(M7-S2) model were found to be 1.92 and 2.32 Å for the Zn–O and Zn–Zn distances, respectively, which are well consistent with the structural data obtained from our EXAFS analysis (Tab. 1). In addition, the UV-vis spectrum reproduced by the time-dependent density functional theory (TD-DFT) calculation using the $[\text{Zn}_2]^{2+}$ -(M7-S2) model showed qualitative agreement with the experimental spectrum (Fig. 2B). The $[\text{Zn}_2]^{2+}$ -(M7-S2) model exhibits two distinct absorption bands in the region of 50,000-30,000 cm^{-1} . The Kohn-Sham molecular orbital evaluated for the $[\text{Zn}_2]^{2+}$ -(M7-S2) model revealed that the ground state of the $[\text{Zn}_2]^{2+}$ unit has a $(\sigma)^2$ electronic structure, and the two distinct absorption bands in TD-DFT spectra are primarily from the σ (doubly occupied orbital) $\rightarrow \sigma^*$ and/or π (vacant orbitals in the original state) transitions for the dimeric $[\text{Zn}_2]^{2+}$ species (Fig. 2C). These reproduce the experimental spectrum well, supporting the formation of $[\text{Zn}_2]^{2+}$ species in the MFI zeolite samples. A discussion on the possibility of another model with different Al array is given in the Supporting Information as the supplementary Figs. S4 and S5. The Zn^{2+} species exchanged on the [M7-S2] site, which exhibit novel activation properties of H_2 as well as CH_4 , in the present MFI-type zeolite sample (Si/Al = 11.9) amount to ca. 20% of the quantity of totally exchanged zinc ion. In addition, as we described the possibility of another model (supporting information: S4 and S5), there are possibilities of dimer formation in other types of sites. Therefore, it is entirely fair to say that the formation of dimeric

zinc-ion species described takes place efficiently in the MFI samples with the Si/Al ratio of ca. 12 or less. Taking these points into consideration, it is not to be denied that the formation of dimer species may be difficult in the zeolite samples with higher value of Si/Al owing to the increase in the distance between Al–Al.

3.3 Proposal for the formation mechanism by making use of the DFT method.

Complexes containing $[\text{Zn}_2]^{2+}$ species have been prepared in other works carried out so far, but these have decomposed easily and disproportionally to form Zn^{2+} and Zn^0 at the temperatures between 298 and 573 K.^{37–41} In contrast to these studies, the XAFS data in the present work evidenced that thermally stable $[\text{Zn}_2]^{2+}$ species were formed utilizing specific reaction field of the MFI zeolite through a comproportionation reaction at higher temperature (at 673 K) between a monomeric Zn^{2+} ion exchanged in the MFI zeolite and a Zn^0 atom inserted in the MFI zeolite. The reverse (disproportionation) reaction, i.e., $[\text{Zn}_2]^{2+} \rightarrow \text{Zn}^{2+} + \text{Zn}^0$, Scheme 1 (c→b), does not occur even at temperatures not greater than 773 K. After treatment at 873 K in vacuo, the sample returns ultimately to its original state, causing the reverse reaction: shown in supplementary Fig. S6 and Table S1. Therefore, we concluded that it is the MFI structure that affords peculiar reaction field which stabilizes the Zn^+-Zn^+ linkage. To substantiate the formation of $[\text{Zn}_2]^{2+}$ species, we attempted to produce the $[\text{Zn}_2]^{2+}$ species with the aid of DFT calculation employing the optimized Zn^{2+} -(M7–S2) model, in which a monomeric Zn^{2+} , $\text{Zn}^{2+}(1)$, was located at the vicinity of two Al atoms in the M7–S2 site, together with a single Zn^0 species, $\text{Zn}^0(2)$. In this calculation, the $\text{Zn}^0(2)$ atom was initially positioned at a distant point located ca. 3.00 Å from the monomeric $\text{Zn}^{2+}(1)$ ion exchanged at the M7–S2 site, and the structure models were then fully optimized (Fig. 3). In Fig. 3, the value of R denotes the bond distance between the two zinc species. Consequently, the Zn^0 atom interacted with the monomeric Zn^{2+} ion at the M7–S2 site to form a $[\text{Zn}_2]^{2+}$ species spontaneously and stably with a significant release of heat (enthalpy of formation ca. -150 kJ mol^{-1}), as shown in Fig. 3A. A natural population analysis of the respective stages in the $[\text{Zn}_2]^{2+}$ formation process revealed that an electron transfer from $\text{Zn}(2)\text{-}4s$ (occupied orbital), Zn^0 , toward $\text{Zn}(1)\text{-}4s$ (unoccupied orbital), Zn^{2+} ,

was the key driving force for the formation of the $[\text{Zn}_2]^{2+}$ species, which clearly demonstrates the occurrence of a simple comproportionation reaction between Zn^0 and Zn^{2+} (Fig. 3B), together with the snapshots of the structure in several stages (Fig. 3C). The important point to note here is that the evaluated energy of the disproportionation reaction for this system ($+150 \text{ kJ mol}^{-1}$) is substantially larger than the corresponding energy for decamethyldizincocene (ca. $+84 \text{ kJ mol}^{-1}$) reported by Xie et al.,²¹ indicating that the $[\text{Zn}_2]^{2+}$ species in the MFI zeolite is thermally stable compared with the similar species in decamethyldizincocene. As a result, all experimental data are explained reasonably using the models proposed in this work; i.e., when a Zn^{2+} ion-exchanged MFI sample is exposed to Zn^0 vapour, $[\text{Zn}_2]^{2+}$ is formed spontaneously through a simple comproportionation reaction between a monomeric Zn^{2+} ion and a Zn^0 atom with the benefit of MFI reaction fields.

3.4. Reactivity of $[\text{Zn}_2]^{2+}$ species formed in MFI and its visualization.

Taking into account of the formation of $[\text{Zn}_2]^{2+}$ species in the MFI zeolite, it is expected that through photoactivation on excitation in the $\sigma \rightarrow \sigma^*$ absorption region, the homo-bimetallic species may undergo homolytic metal-metal bond cleavage, which has the potential to lead to unique catalytic behaviour.^{42,43} However, so far, no one has succeeded in such activation in analogous zinc compounds, and the photochemistry of $[\text{Zn}_2]^{2+}$ has remained essentially unexplored. Here, to deepen our understanding of the characteristic photochemical reactivity of the $[\text{Zn}_2]^{2+}$ species in the MFI zeolite, its response to UV light irradiation was examined under vacuum conditions. The UV-vis DR and ESR spectra of Sample HMFI- Zn^0 -15 before and after irradiation with light in the wavenumber region of $50,000\text{-}30,000 \text{ cm}^{-1}$ are shown in Figs. 4A and B. Upon UV irradiation, the intensity of the DR band at $50,000\text{-}30,000 \text{ cm}^{-1}$ attributed to the $[\text{Zn}_2]^{2+}$ species decreased slightly, accompanied by the appearance of new DR bands at $36,000$ and $32,750 \text{ cm}^{-1}$. In addition, a distinct isotropic ESR signal appeared at $g = 1.9980$, ascribed to the paramagnetic Zn^+ species.¹⁴ It follows from what has been said that this change initiated by irradiation with light in the wavenumber region $50,000$ to $35,000 \text{ cm}^{-1}$ corresponds to the $\sigma \rightarrow \sigma^*$ excitation energy of the $[\text{Zn}_2]^{2+}$ species (Fig. S7). The photoinduced $\sigma \rightarrow \sigma^*$ transition of the $[\text{Zn}_2]^{2+}$ species reduces the bond order of Zn^+-Zn^+ from one

to zero, which leads to the photolytic cleavage of the Zn^+-Zn^+ linkage, resulting in the formation of two paramagnetic Zn^+ ions that are then captured stably at the ion-exchangeable sites in the MFI zeolite, as shown in Scheme 1 (c \rightarrow d). It should be noted that heating the UV irradiated sample at 573 K brought about the recombination of two discrete Zn^+ ions (Scheme 1 (c \leftarrow d)), as evidenced by full recovery of the intensity of the DR band attributed to the $[\text{Zn}_2]^{2+}$ species, resulting in a decrease in intensity of both the DR and ESR bands because of the paramagnetic Zn^+ species: Figs. 4A and B. It cannot be emphasized too strongly that this is the first example of the observation of a reversible cleavage and recombination of an original Zn^+-Zn^+ bond in the MFI zeolite: see Scheme 1 (c \rightleftharpoons d). This fact indicates that we are able to control and manipulate the magnetic property of Zn^+ at the atomic-level by utilizing an MFI zeolite as the reaction field.

Thus far, there are no successful examples of the detection of the metal radical centres photo-generated through the photolytic cleavage of the homonuclear metal-metal bond even at ambient temperature, because the metal radical species formed are so active that they react quickly with the surrounding molecules. In the present case, the photolysis of the $[\text{Zn}_2]^{2+}$ species formed at the specific site in the MFI zeolite gave stable paramagnetic Zn^+ ions. The MFI zeolite with an appropriate configuration of Al atoms affords a suitable and specific reaction field for stabilizing two types of monovalent zinc ions; namely dimer ($[\text{Zn}_2]^{2+}$), as well as Zn^+ monomer ions. This unusual phenomenon can be explained by considering that the sites in the MFI zeolite make two local potential energy minima at short and at long Zn^+-Zn^+ distances, separated by an unambiguous energy barrier between them, as shown in Scheme 2.

3.5. Evaluation of the mechanism in the reversible changing process between $[\text{Zn}_2]^{2+}$ and 2Zn^+ .

To confirm the idea described just above, DFT calculation was applied to the present system. In these calculations, we first analyzed the potential energy surfaces for the singlet and triplet states of the $[\text{Zn}_2]^{2+}$ -(M7-S2) model as a function of the Zn-Zn separation by assuming the formation of a zinc species having the singlet spin state (one $[\text{Zn}_2]^{2+}$ composed of $[\text{Zn}^+-\text{Zn}^+]$) and two zinc species with the doublet spin states (two paramagnetic Zn^+ ions: totally triplet state). Reasonable potential

energy surfaces were obtained as a result (Fig. 5). The reproduced potential energy surfaces for the singlet ground and triplet excited states of the $[\text{Zn}_2]^{2+}$ -(M7-S2) model show local minima at short and long Zn–Zn lengths (at 2.33 and 4.01 Å, respectively), with intercrossing potential functions between singlet and triplet states. These calculation data can be explained as follows. When the excited $[\text{Zn}_2]^{2+}$ triplet state is formed at the M7-S2 site on UV activation, it relaxes spontaneously to a state having a long Zn–Zn distance of 4.01 Å; i.e., two paramagnetic Zn^+ ions are formed in the metastable state, and they are captured stably on respective ion-exchangeable sites in the MFI zeolite at an ambient temperature. A definite energy barrier between triplet and singlet states of the dimeric species is generated at the intersection of the potential energy surfaces for the singlet and triple states at around 3.90 Å. The relaxation process requires some external energy to be able to overcome the energy barrier (calculated to be ca. 10 kJ/mol) at the intercrossing point. As a result, the energy calculation data explain the experimental facts well that stable Zn^+ species are formed at room temperature, but a recombination reaction ($2 \text{Zn}^+ \rightarrow \text{Zn}^+-\text{Zn}^+$) occurs at higher temperatures (ca. 573 K). Therefore, we concluded that the specific site in the MFI zeolite with appropriate Al–Al distance has the potential to create two types of Zn^+ species made up of two Zn^+ ions: diamagnetic $[\text{Zn}_2]^{2+}$ and two paramagnetic Zn^+ ions.

4. Conclusion

In summary, the work presented here provides unprecedented insights about the synthesis and nature of unusual Zn^+ by utilizing the subnanometer sized space of the MFI zeolite as a reaction pot. Exposure of the HMFI zeolite to Zn^0 vapour under the condition including Zn^0 in small amounts at 673 K selectively made up of a monomeric Zn^{2+} ion-exchanged in MFI. As the Zn^0 loading increases, thermally stable $[\text{Zn}_2]^{2+}$ was formed through a spontaneous reverse disproportionation reaction between the monomeric Zn^{2+} ions exchanged in MFI and enough amounts of vapourized Zn^0 . Photolysis under UV irradiation in the σ - σ^* absorption region of the $[\text{Zn}_2]^{2+}$ species formed in the MFI zeolite converted it into two paramagnetic Zn^+ ions in a stable state. The photo-generated two paramagnetic Zn^+ species recombined to form the original $[\text{Zn}_2]^{2+}$ species on heating to 573 K in vacuo; the formation of the $[\text{Zn}_2]^{2+}$ species and the homolysis of the Zn^+-Zn^+ bond were realized

using the specific reaction field of the MFI zeolite with the characteristic Al arrangement. The mechanism of the reversible bond cleavage and formation can be explained by assuming the existence of the specific sites with the peculiar Al array in the MFI zeolite making two local minima at short and long Zn^+-Zn^+ distances, with a definitive barrier between the minima. The findings in this study highlight not only new Zn^+ ion chemistry but also the potential of using of the MFI zeolite reaction field to create fascinating metal species endowed with the switchable magnetic property onto Zn^+ ions.

Acknowledgement

Financial supports were provided by Japan Society of Promotion Science (Grants-in-Aid for Scientific Research: No. 21655021). XAFS measurements were performed under the proposal No's of 2011G538 and 2012G597 of the Photon Factory Advisory Committee. We thank Prof. M. Nomura, Dr. H. Nitani, and Dr. A. Koyama at PF in Tsukuba for their kind assistance in acquiring the XAFS spectra. A.O. of authors acknowledges his financial support from Japan Society for the Promotion of Science (Research Fellowship for Young Scientists, DC1).

Author contributions

A.O. carried out the experiments and theoretical works, and also contributed to the writing process of the manuscript. T.O. did a great deal for the experimental works and T.Y. and H.K. contributed to the theoretical works, and all authors also participated in the discussion of the results. Y.K. designed and directed the research, and contributed to the preparation and writing of the manuscript. All authors reviewed the manuscript.

Notes and references

¹*Department of Chemistry, Graduate School of Natural Science and Technology, Okayama University, 3-1-1 Tsushima, Kita-ku, Okayama 700-8530, Japan.*

²*Department of Chemistry and Materials Technology, Kyoto Institute of Technology, Matsugasaki,*

Sakyo-ku, Kyoto 606-8585, Japan.

*E-mail: kuroda@cc.okayama-u.ac.jp (Y.K.)

† Electric Supplementary Information (ESI) available: [Supporting information is available in the online version of the paper](#). See DOI: 10.1039/b00000000000/.

- [1] N. N. Greenwood, A. Earnshaw, *Chemistry of the Elements* (Butterworth-Heinemann: Burlington, 2nd ed., 1997).
- [2] P. J. Hay, J. C. Thibault, R. Hoffmann, *J. Am. Chem. Soc.* 1975, **97**, 4388–4403.
- [3] P. K. Mehrotra, R. Hoffmann, *Inorg. Chem.* 1978, **17**, 2187–2189.
- [4] N. E. Schultz, Y. Zhao, D. G. Truhlar, *J. Phys. Chem. A* 2005, **109**, 4388–4403.
- [5] P. N. Moorthy, J. J. Weiss, *Nature* 1964, **201**, 1317–1318.
- [6] J.-I. Isoya, S. Fujiwara, *Bull. Chem. Soc. Jpn.* 1972, **45**, 2182–2188.
- [7] F. F. Popescu, V. V. Grecu, 1973, **13**, 749–751.
- [8] J. Xu, A. Zheng, X. Wang, G. Qi, J. Su, J. Du, Z. Gan, J. Wu, W. Wang, F. Deng, *Chem. Sci.* 2012, **3**, 2932–2940.
- [9] I. Resa, E. Carmona, E. Gutierrez-Puebla, A. Monge, *Science* 2004, **305**, 1136–1138.
- [10] T. Li, S. Schulz, P. W. Roesky, *Chem. Soc. Rev.* 2012, **41**, 3759–3771.
- [11] C. E. Housecroft, A. G. Sharpe, *Inorganic Chemistry* 3rd ed. Person Education Limited, Harlow, England, 2008.
- [12] A. Oda, H. Torigoe, A. Itadani, T. Ohkubo, T. Yumura, H. Kobayashi, Y. Kuroda, *Angew. Chem. Int. Ed.* 2012, **51**, 7719–7723.
- [13] A. Oda, H. Torigoe, A. Itadani, T. Ohkubo, T. Yumura, H. Kobayashi, Y. Kuroda, *J. Phys. Chem. C* 2013, **117**, 19525–19534.
- [14] A. Oda, H. Torigoe, A. Itadani, T. Ohkubo, T. Yumura, H. Kobayashi, Y. Kuroda, *J. Am. Chem. Soc.* 2013, **135**, 18481–18489.
- [15] T. Taguchi, T. Ozawa, H. Yashiro, *Physica Scripta* 2005, **T115**, 205–206.

- [16] Gaussian 09, Revision **D.01**, M. J. Frisch, G. W. Trucks, H. B. Schlegel, G. E. Scuseria, M. A. Robb, J. R. Cheeseman, G. Scalmani, V. Barone, B. Mennucci, G. A. Petersson, H. Nakatsuji, M. Caricato, X. Li, H. P. Hratchian, A. F. Izmaylov, J. Bloino, G. Zheng, J. L. Sonnenberg, M. Hada, M. Ehara, K. Toyota, R. Fukuda, J. Hasegawa, M. Ishida, T. Nakajima, Y. Honda, O. Kitao, H. Nakai, T. Vreven, J. A. Montgomery, Jr., J. E. Peralta, F. Ogliaro, M. Bearpark, J. J. Heyd, E. Brothers, K. N. Kudin, V. N. Staroverov, R. Kobayashi, J. Normand, K. Raghavachari, A. Rendell, J. C. Burant, S. S. Iyengar, J. Tomasi, M. Cossi, N. Rega, J. M. Millam, M. Klene, J. E. Knox, J. B. Cross, V. Bakken, C. Adamo, J. Jaramillo, R. Gomperts, R. E. Stratmann, O. Yazyev, A. J. Austin, R. Cammi, C. Pomelli, J. W. Ochterski, R. L. Martin, K. Morokuma, V. G. Zakrzewski, G. A. Voth, P. Salvador, J. J. Dannenberg, S. Dapprich, A. D. Daniels, Ö. Farkas, J. B. Foresman, J. V. Ortiz, J. Cioslowski, D. J. Fox, Gaussian, Inc., Wallingford CT, 2009.
- [17] A. D. Becke, *Phys. Rev.* 1988, **A38**, 3098–3100.
- [18] A. D. Becke, *J. Chem. Phys.* 1993, **98**, 5648–5652.
- [19] P. J. Stephens, F. J. Devlin, C. F. Chabalowski, M. J. Frisch, *J. Phys. Chem.* 1994, **98**, 11623–11627.
- [20] C. Lee, W. Yang, R. G. Parr, *Phys. Rev.* 1988, **B37**, 785–789.
- [21] I. N. Levine, *Quantum Chemistry V. ed.*, Prentice Hall, Inc., Upper Saddle River, New Jersey. **1999**.
- [22] T. Yumura, M. Takeuchi, H. Kobayashi, Y. Kuroda, *Inorg. Chem.* 2009, **48**, 508–517.
- [23] The MFI structure was taken from the Cerius 2 data base: Accelrys Software, Inc., San Diego, CA.
- [24] A. Itadani, H. Sugiyama, M. Tanaka, T. Ohkubo, T. Yumura, H. Kobayashi, Y. Kuroda, *J. Phys. Chem. C* **2009**, *113*, 7213–7222.
- [25] T. Yumura, H. Yamashita, H. Torigoe, H. Kobayashi, Y. Kuroda, *Phys. Chem. Chem. Phys.* 2010, **12**, 2392–2400.
- [26] A. Itadani, T. Yumura, T. Ohkubo, H. Kobayashi, Y. Kuroda, *Phys. Chem. Chem. Phys.* 2010, **12**, 6455–6465.

- [27] A. Itadani, M. Tanaka, T. Mori, H. Torigoe, H. Kobayashi, Y. Kuroda, *J. Phys. Chem. Lett.* 2010, **1**, 2385–2390.
- [28] H. Torigoe, T. Mori, K. Fujie, T. Ohkubo, A. Itadani, K. Gotoh, H. Ishida, H. Yamashita, T. Yumura, H. Kobayashi, Y. Kuroda, *J. Phys. Chem. Lett.* 2010, **1**, 2642–2650.
- [29] T. Yumura, T. Nanba, H. Torigoe, Y. Kuroda, H. Kobayashi, *Inorg. Chem.* 2011, **50**, 6533–6542.
- [30] A. Oda, H. Torigoe, A. Itadani, T. Ohkubo, T. Yumura, H. Kobayashi, Y. Kuroda, *J. Phys. Chem. C* 2014, **118**, 15234–15241.
- [31] T. Yumura, A. Oda, H. Torigoe, A. Itadani, Y. Kuroda, T. Wakasugi, H. Kobayashi, *J. Phys. Chem. C* 2014, **118**, 23874–23887.
- [32] D. Nachtigalová, P. Nachtigall, M. Sierka, J. Sauer, *Phys. Chem. Chem. Phys.* 1999, **1**, 2019–2026.
- [33] D. Grandjean, V. Pelipenko, E. D. Batyrev, J. C. van den Heuvel, A. A. Khassin, T. M. Yurieva, B. M. Weckhuysen, *J. Phys. Chem. C* 2011, **115**, 20175–20191.
- [34] F. Rittner, A. Seidel, B. Boddenberg, *Microporous Mesoporous Mater.* 1998, **24**, 127–131.
- [35] D. Río, A. Galindo, I. Resa, E. Carmona, *Angew. Chem. Int. Ed.* 2005, **44**, 1244–1247.
- [36] Z. Zhu, R. J. Wright, M. M. Olmstead, E. Rivard, M. Brynda, P. P. Power, *Angew. Chem. Int. Ed.* 2006, **45**, 5807–5810.
- [37] Y. Xie, Y. H. F. Schaefer III, R. B. King, *J. Am. Chem. Soc.* 2005, **127**, 2818–2819.
- [38] A. Schnepf, H.-J. Himmel, *Angew. Chem. Int. Ed.* 2005, **44**, 3006–3008.
- [39] A. Grirrane, I. Resa, A. Rodríguez, E. Carmona, E. Alvarez, E. Gutierrez-Puebla, A. Monge, A. Galindo, D. del Rio, R. A. Andersen, *J. Am. Chem. Soc.* 2007, **129**, 693–703.
- [40] E. Carmona, A. Galindo, *Angew. Chem. Int. Ed.* 2008, **47**, 6526–6536.
- [41] A. Grirrane, I. Resa, A. Rodríguez, E. Carmona, *Coord. Chem. Rev.* 2008, **252**, 1532–1539.
- [42] M. S. Wrighton, D. Ginley, *J. Am. Chem. Soc.* 1975, **97**, 2065–2072.
- [43] M. K.; Reinking, M. L. Kullberg, A. R. Cutler, C. P. Kubiak, *J. Am. Chem. Soc.* 1985, **107**, 3517–3524.

Figure captions

Fig. 1. XAFS and UV spectra of HMFI-Zn⁰-X samples. (A) XANES and (B) Fourier transforms of the EXAFS oscillations at the Zn K-edge of the HMFI-Zn⁰-X samples with different Zn⁰ loadings. (C) The relation between coordination numbers evaluated for the 2nd nearest band from EXAFS spectra and the band intensities observed at 9660.7 eV in XANES spectra was plotted for respective samples: X= 5, 7.5, 10 and 15. (D) UV-DR spectra of respective samples.

Fig. 2. (A) The optimized structure of the [Zn₂]²⁺ species positioned on the M7-S2 site in MFI. (B) Experimentally (dashed line) obtained UV spectrum of the HMFI-Zn⁰-15 sample, and theoretically obtained components, as well as spectrum (red solid line), by applying TD-DFT calculation method to the model shown in (A), together with their respective components bands. In the calculation of the spectrum by the TD-DFT method, the FWHM of the reproduced spectrum was set to 2,000 cm⁻¹. (C) Their respective components corresponding to each transition from σ to σ^* , π_x , and π_y , were given. The colors depicted by arrows in (C) correspond to the components given in (B).

Fig. 3. (A) The changes in the stabilization energies and (B) in electron densities with the distance between Zn(1) and Zn(2) in the optimization processes, and (C) the snapshots of the structural changes in the optimization processes as a function of the Zn(1)-Zn(2) distance.

Fig. 4. In situ UV-vis DR and ESR spectra for the HMFI-Zn⁰-15 sample in various conditions. (A) The UV-vis DR and (B) ESR spectra for the HMFI-Zn⁰-15 sample: (1) before and (2) after UV irradiation, and (3) followed by successive heating at 573 K. In Fig. 4A, the difference spectrum between (1) and (2), (solid orange line), was also given.

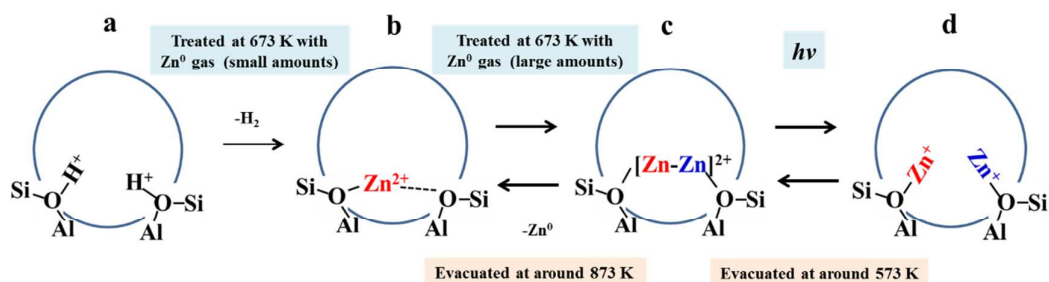
Fig. 5. DFT studies on the reversible homolysis and recombination of the Zn⁺-Zn⁺ bond in the [Zn₂]²⁺ species formed in MFI. (A), The potential energy surfaces of the singlet and triplet states of the formed [Zn₂]²⁺ in the M7-S2 site as a function of the Zn-Zn distance. (B), The optimized structure for the triplet state comprised of the Zn⁺-Zn⁺ pair having bond distance of 4.01 Å in which the Zn⁺-Zn⁺ bond is completely ruptured.

Table 1. Structural parameters obtained from EXAFS analysis of the HMFI-Zn⁰-X samples.

Sample	1st shell			2nd shell		
	$N_{\text{Zn-O}}$	$R_{\text{Zn-O}}$	$\sigma^2_{\text{Zn-O}}$	$N_{\text{Zn-Zn}}$	$R_{\text{Zn-Zn}}$	$\sigma^2_{\text{Zn-Zn}}$
HMFI-Zn ⁰ -5	2.7	1.93	0.011	0.3	2.35	0.012
HMFI-Zn ⁰ -7.5	2.7	1.93	0.011	0.6	2.34	0.010
HMFI-Zn ⁰ -10	2.4	1.94	0.012	0.8	2.38	0.009
HMFI-Zn ⁰ -15	2.3	1.94	0.013	1.1	2.37	0.009

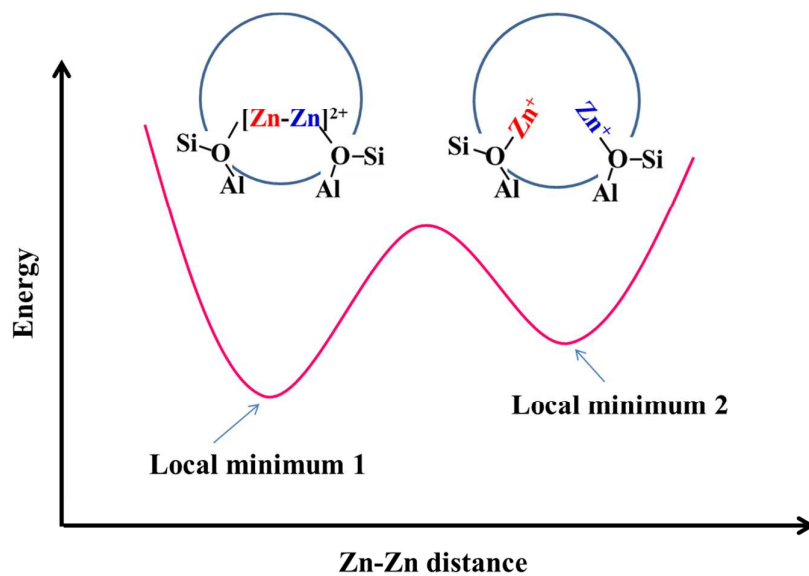
Table 1. Structural parameters for the 1st and 2nd shells which were obtained by the EXAFS analysis for respective HMFI-Zn⁰-X samples: where N , coordination number; R , distance in Å; σ^2 , Debye-Waller factor in Å².

Scheme 1. A. Oda et al.,



Scheme 1. Summarized schematic views for the proposed reaction processes including the formation of the $[\text{Zn}_2]^{2+}$ species caused by the reaction between HMFIs and Zn^0 vapour, as well as the bond dissociation process of the $[\text{Zn}_2]^{2+}$ species.

Scheme 2. A. Oda et al.,



Scheme 2. Schematic view of the potential surface models corresponding to each equilibrium step:
 $[\text{Zn}_2]^{2+} \rightleftharpoons 2\text{Zn}^+$

Figure 1. A. Oda et al.,

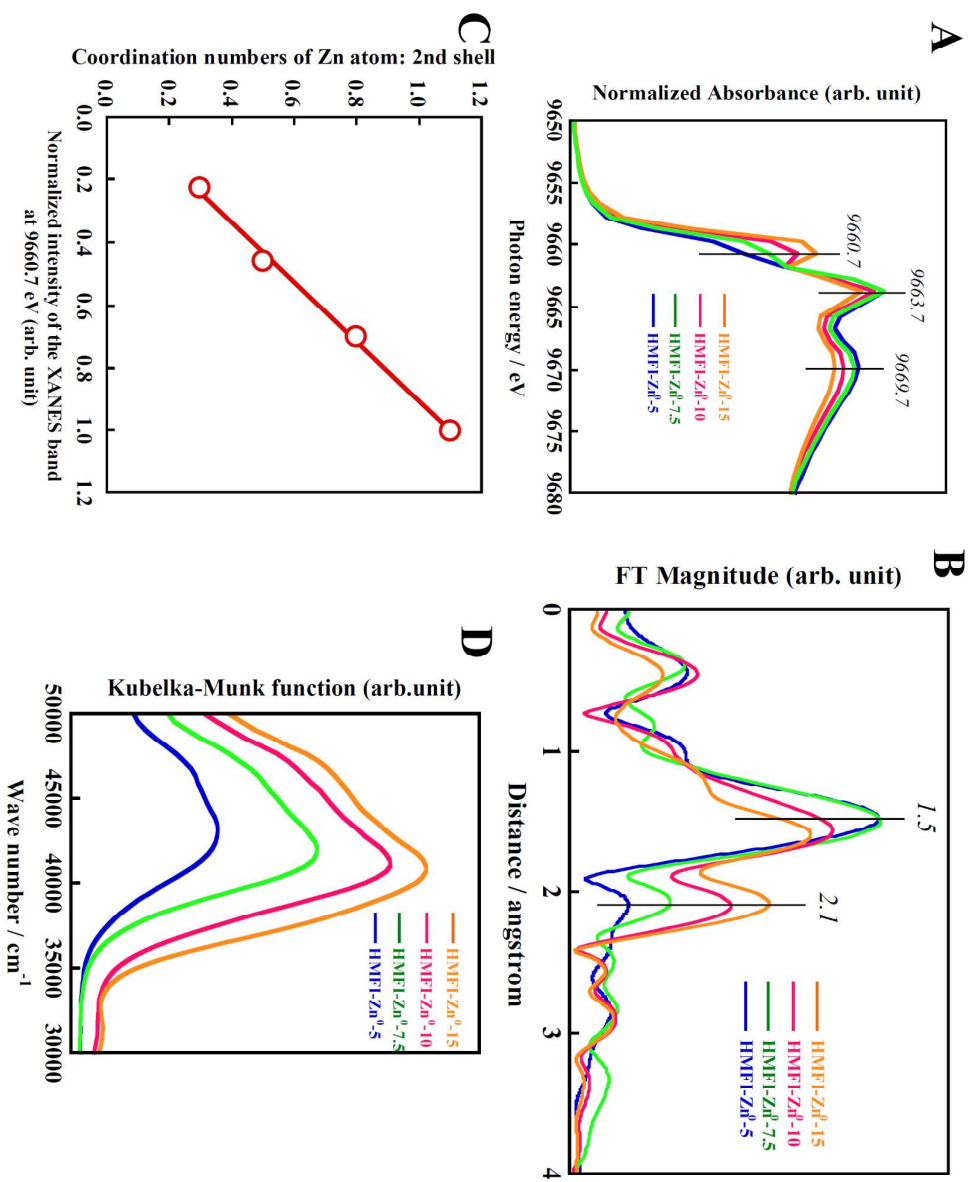


Figure 2. A. Oda et al.,

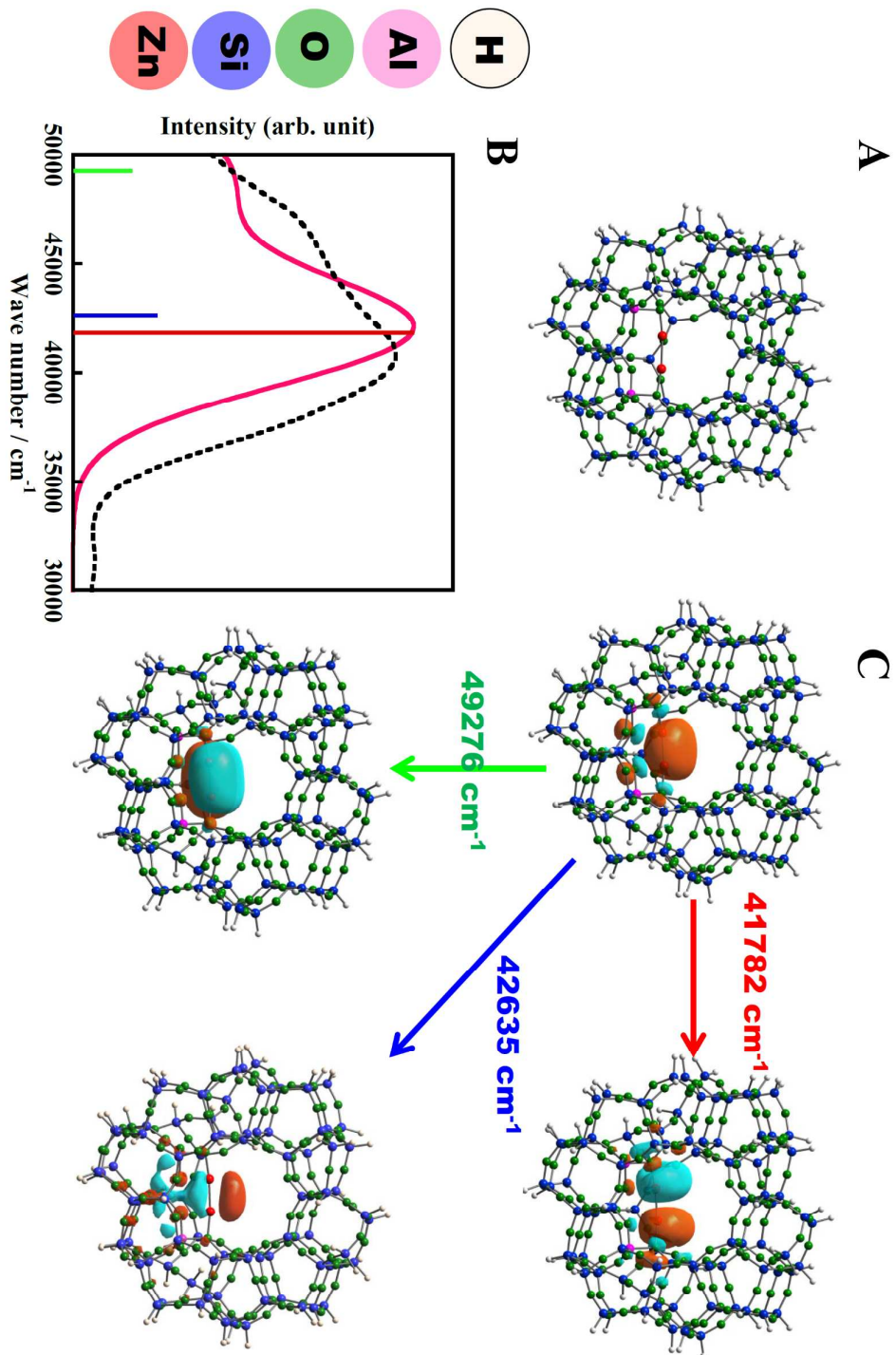


Figure 3. A. Oda et al.,

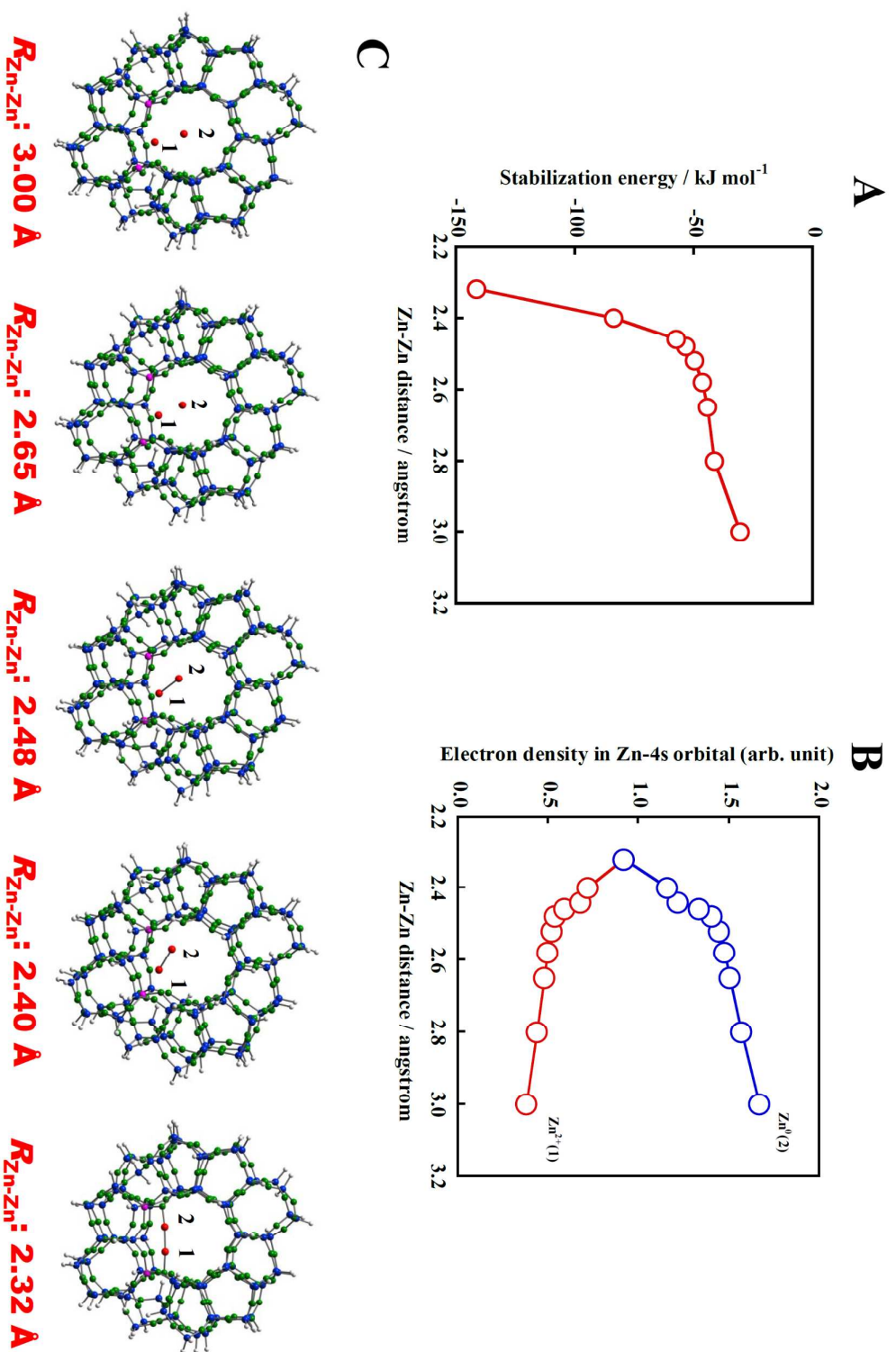


Figure 4. A. Oda et al.,

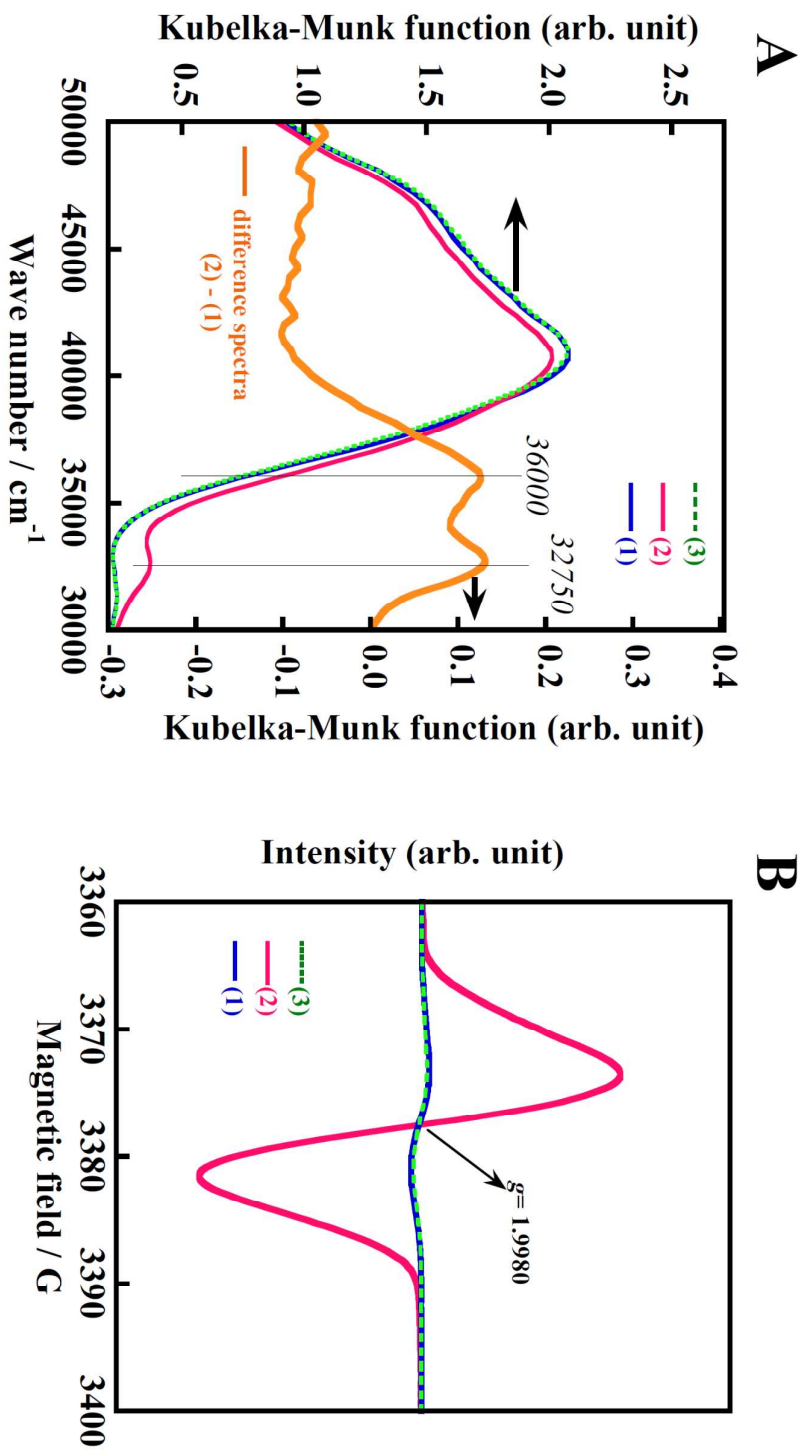


Figure 5. A. Oda et al.,

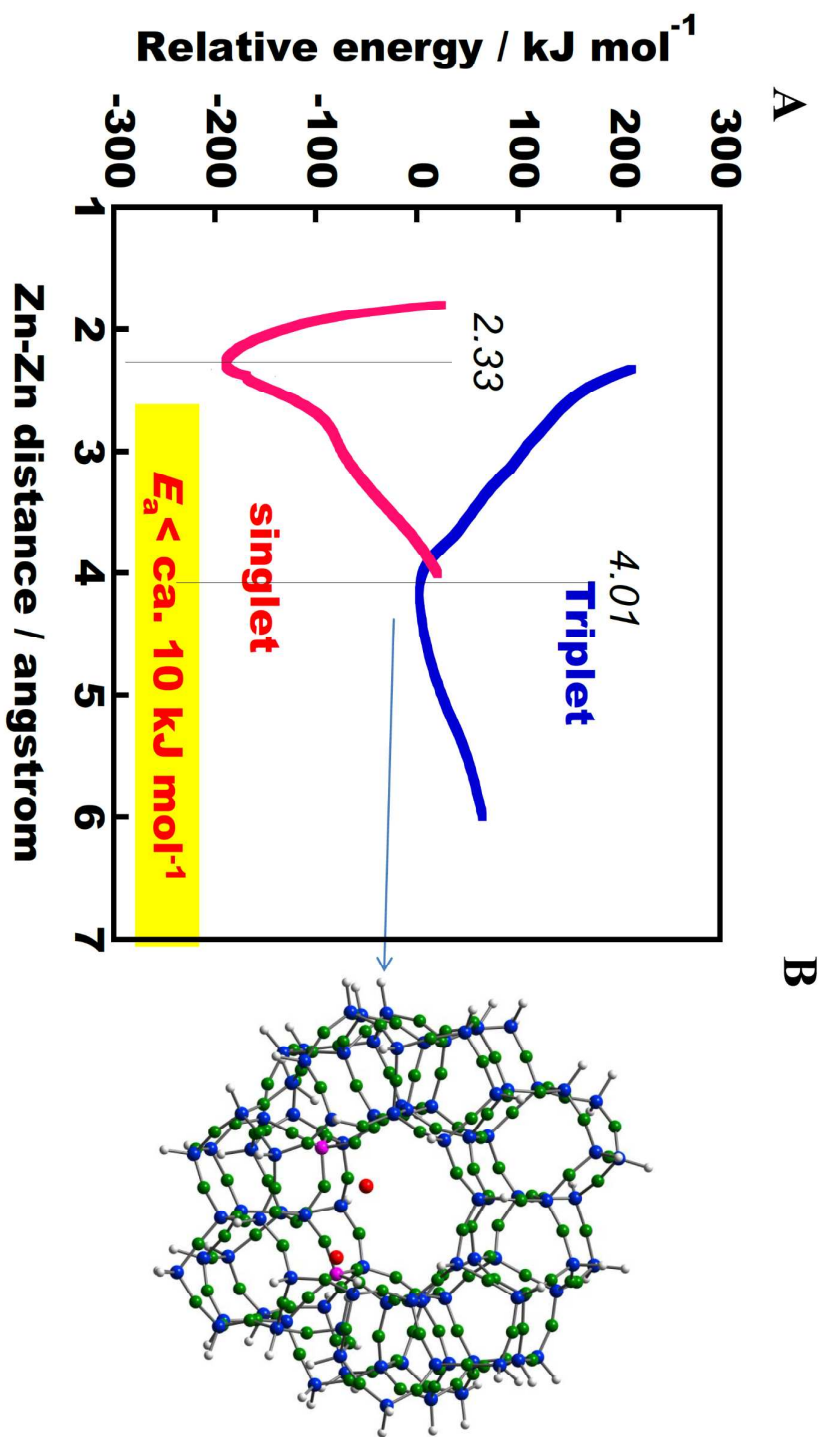
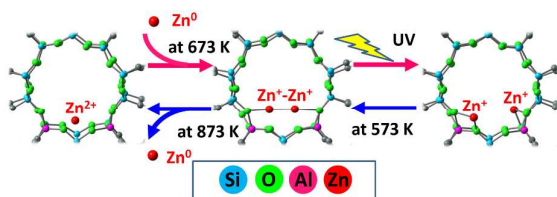


Table of content



Specific-field emanating from zeolite with specific Al-array makes it possible to synthesize the “ultra-state ion, $[Zn_2]^{2+}$ ” and to manipulate between dimer and monomer with light and heat.